한국공작기계학회 2002 춘계학술대회 논문집 pp. 255~260

밀링 작업에서 순간 전단면에 기초한 절삭력 모델에 관한 연구
A Study on the Instantaneous Shear Plane Based Cutting Force Model for End Milling

홍 민 성/ 아주대학교 공과대학 기계공학부
Min-Sung Hong/Div. of Mech. Eng., Ajou University

ABSTRACT

The purpose of this paper is to further extend the theoretical understanding of the dynamic end milling process and to derive a computational model to predict the milling force components. A comparative assessment of different cutting force models is performed to demonstrate that the instantaneous shear plane based formulation is physically sound and offers the best agreement with experimental results. The procedure for the calculation of the model parameters used in the cutting force model, based on experimental data, has been presented. The validity of the proposed computational model has been experimentally verified through a series of cutting tests.

1. INTRODUCTION

A disadvantage apparent from the overview of recent metal removal research is the lack of a compelling physical reason for modeling and predicting cutting forces as being proportional to the undeformed chip cross section area or the combination of the instantaneous depth of cut and penetration rate in particular under dynamic cutting conditions. As it is well established by examination of photomicrographs of a partially formed chip the material is deformed by a shearing process along the shear zone/plane (Shaw, 1991). The material deformation rate is very high along the shear plane as a consequence of a very thin region in which shear occurs. In this sense, the cutting force components should have been associated with the area of the shear plane. However, the shear plane area is difficult to calculate since its direction is affected by the instantaneous cutting velocity, which is also a function of time, and also by the machined surface cut in a previous tool pass. Therefore, the concept that the chips are sheared from the workpiece is well perceived but seldom used in machining performance prediction.

The need for quantitative machining performance information has been recognized by many researchers and also by industry (Shin and Waters, 1994, Armarego et al., 1995). Due to the wide variety of machining operations and numerous factors influencing each operation the development of models for the prediction of machining performance represents a formidable task. Because of the complexity of calculations many researchers have used the undeformed chip thickness model to predict cutting forces. This is basically due to the difficulty of measuring the length of the shear line and to represent it as a function of measurable variables such as the undeformed chip thickness, vibration velocity, and accelerations. As a consequence, the linear force model that proportionally relates the undeformed chip thickness to the cutting force is widely used in analysis and simulation models.

To achieve a more accurate prediction of dynamic force components the physically more adequate and meaningful approach to the evaluation and simulation of the dynamic cutting processes, based on the consideration of the dependence of the dynamic cutting forces on the instantaneous shear plane area, will be adopted. Therefore, in this paper a cutting force model for end milling operations based on the instantaneous shear plane will be derived and experimentally verified.

2. CUTTING FORCE MODELS IN MILLING

Many past efforts have concentrated on the analysis of general three-dimensional cutting mechanics for oblique cutting. Shaw et al. (1952) analyzed oblique cutting and introduced the effective rake and effective shear angles by treating the material flow in three-dimensional cutting as modification of the plane strain model of orthogonal cutting.

It is generally assumed that the shear plane keeps a constant direction in space though it is well known that the shear plane is varying in a way not yet fully understood. In early studies, Merchant (1944) and Lee and Shafer (1951) have proposed a shear angle expression as a function of the difference between the mean angle of friction on the tool face β and the rake angle γ:

$$\phi = c_1 + c_2(\beta - \gamma) \quad (1)$$

where c_1 and c_2 are constant coefficients. This expression is based on the assumption that the shear angle depends on the mean angle of friction on the tool surface.

2.1 Comparison of Different Force Models

There are numerous algorithms for estimating cutting forces by considering cutting forces as a function of the:

(A) instantaneous shear plane area,
(B) nominal undeformed chip cross section area,
(C) instantaneous undeformed chip cross section area,
(D) nominal undeformed chip cross section area and a penetration rate term.

In order to assess the quantitative and qualitative differences between the four models a numerical approach was adopted. For this purpose, a computer program was written to calculate the non-dimensional cutting force, $f_c(t)$, and thrust force, $f_t(t)$, for the orthogonal cutting process which are defined as:

$$f_c(t) = \frac{F_c(t)}{-b\tau c} \tag{2a}$$

$$f_t(t) = \frac{F_t(t)}{-b\tau c} \tag{2b}$$

where $F_c(t)$ and $F_t(t)$ are the cutting and thrust forces, b and c are the width of cut and the mean undeformed chip thickness, and τ is the average shear stress on the shear plane, respectively.

For the shear plane based model (designated as model A) $F_c(t)$ and $F_t(t)$ can be represented, based on Merchant's (1944) orthogonal cutting force model, as:

$$F_c(t) = \frac{bl(t)\tau\cos(\beta-\gamma)}{\cos(\phi+\beta-\gamma)} \tag{3a}$$

$$F_t(t) = \frac{bl(t)\tau\sin(\beta-\gamma)}{\cos(\phi+\beta-\gamma)} \tag{3b}$$

where $l(t)$ is the length measured from the cutting edge to the free surface along the direction which is tilted at an angle ϕ to the nominal cutting velocity $\bar{V}_n(t)$, and ϕ, β, and γ are the shear, friction, and rake angles respectively.

The undeformed chip cross-section area model, which is widely used in modeling metal cutting operations, can be expressed as (model B) (Tlusty and Ismail, 1983):

$$F_c(t) = -k_c A = -bk_c g(t) \tag{4a}$$

$$F_t(t) = -k_d A = -bk_d g(t) \tag{4b}$$

where $g(t)$ is perpendicular to $\bar{V}_n(t)$, k_c is the cutting stiffness given by $k_c = \tau/\sin\phi$, and k_d is a parameter which depends on the workpiece material for mild steel $k_d = 0.3 \cdot k_c$.

For the instantaneous undeformed chip cross section area based model, which is the extension of the instantaneous undeformed chip thickness model, can be expressed as (model C):

$$F_c(t) = -k_c A_c = -bk_c h(t) \tag{5a}$$

$$F_t(t) = -k_d A_c = -bk_d h(t) \tag{5b}$$

where $h(t)$ is perpendicular to $\bar{V}(t)$. For comparison purposes the values for k_c and k_d used in Eqs. 4 and 5 will be assumed the same.

To rectify this shortcoming of the above two models and to bring the model predictions closer to physical reality and agreement with experimental results a penetration rate term is generally added to the model given by Eq. 4 (Minis et al., 1990, Tobias, 1965) to yield (model D):

$$F_c(t) = -bk_c g(t) - bb_c \dot{g}(t) \tag{6a}$$

$$F_t(t) = -bk_d g(t) - bb_d \dot{g}(t) \tag{6b}$$

where b_c and b_d represent the damping in the cutting and thrust directions, respectively.

The comparison between these models will be discussed with respect to different physical parameters to show the characteristics of different models in the following subsections.

Influence of Phase Shift

Figure 1 shows the non-dimensional cutting and thrust forces, $f_c(t)$ and $f_t(t)$, versus the non-dimensional length, x/λ, for the four models, where x is the coordinate of the cutting edge and where $y_1 = a \cdot \sin(2\pi x/\lambda)$ and $y_2 = c + a \cdot \sin(2\pi x/\lambda + \psi)$ are used to model the cutting waves, i.e., the inner and outer modulations respectively. In these simulations c = 1, k_d/k_c = 0.3, and the simulation range for x is 0 to 2π. The shear plane model is nonlinear when $\bar{V}(t) \neq$ *constant* because of the phase shift term implicitly contained in the shear line length. Model A is generally in phase with models C and D but not with model B which means that models C and D also contain the nonlinear phase shift term because the magnitude and the direction of the force defined by model C is affected by $\bar{V}(t)$ and the penetration rate term in model D implicitly contains the nonlinear phase shift term. The shapes of the cutting and thrust forces are affected by the phase shift between y_1 and y_2 as evidenced by Fig. 1.

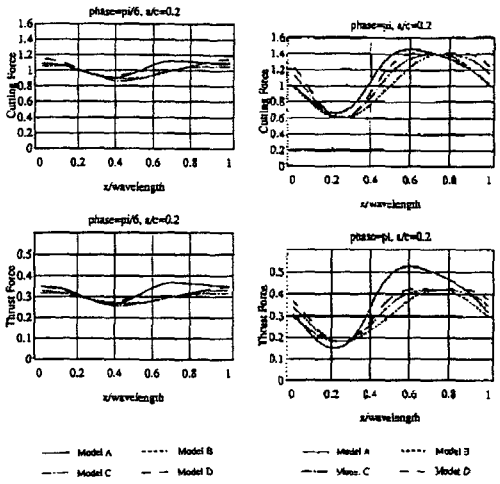

(a) (b)

Fig. 1 Comparison of Different Cutting Force Models (a) $a/c = 0.2, \varphi = \pi/6$ and (b) $a/c = 0.2, \varphi = \pi$

Influence of Vibration Amplitude

Considering conditions with larger vibration amplitudes, shown in Fig. 2, the shapes of the cutting and thrust force components for model A have significantly changed. The differences between model A and the other three models becomes more pronounced for larger vibration amplitudes when compared with Fig. 2.

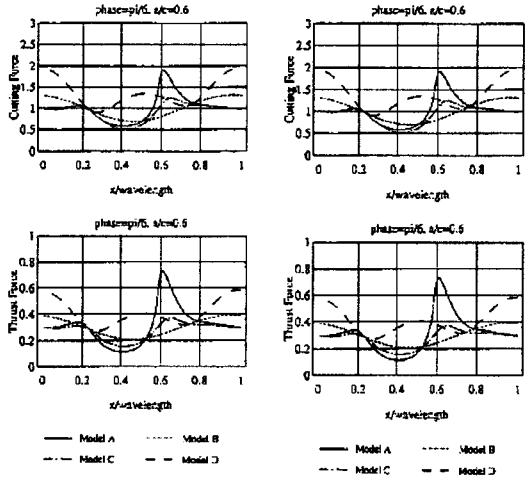

Fig. 2 Comparison of Different Cutting Force Models (a) $a/c = 0.6, \varphi = \pi/6$ and (b) $a/c = 0.6, \varphi = \pi$

Influence of Cutting Velocity

The forces calculated by using models B, C, and D become identical when the cutting velocity $\bar{V}(t)$ = constant ($y_1 = 0$), which corresponds to the case of wave removal (outer modulation). However, the shear plane model (model A) still exhibits a nonlinear property with respect to the undeformed chip thickness that distinguishes it from the other three models. Therefore, the use of models B and D for cutting force calculations might lead to poor results for certain cutting conditions and may prevent a clear physical insight into the mechanisms of the material removal process.

Influence of Vibration Frequency

When machining in the presence of high frequency, low amplitude vibrations the penetration rate term in Eq. 6 (model D) will become the dominant term in calculating the cutting forces and the calculated forces will show large deviations from experimental results. This anomaly of model D corresponds to wave removal with $y_1 = 0$ and $y_2 = c + a \cdot \sin(20\pi x/\lambda)$ in which a vibration frequency ten times higher than that in Fig. 1 is used. The forces calculated by using model D are much larger than the force components calculated by the other cutting force models.

Based on the aforementioned comparisons and discussions the obvious differences between the non-dimensional forces generated by different cutting force models were indicated. The penetration rate model (model D) yields unreasonable results for high frequency wave removal machining. The nominal cutting area based model (model B) cannot adequately reflect the phase shift's effect due to its proportional nature. The results generated by the instantaneous undeformed chip cross section area model (model C) are close to the shear plane model for certain conditions because they are related to the instantaneous cutting velocity. The shear plane based cutting force model is physically more reasonable and in better agreement with observations (Shaw, 1991, Usui, et al., 1978, Armarego and Epp, 1970). Finally, the computational load for model C is approximately equal to that of model A. There is virtually no experimental evidence in support of concept C in previous research.

Therefore, to improve the analysis of milling operations one major goal of this research is to derive a shear plane based cutting force model and the associated algorithms to effectively calculate the instantaneous shear plane area to predict the cutting forces.

3. SHEAR PLANE BASED CUTTING FORCE MODEL FOR END MILLING OPERATIONS

The starting point of the analysis will rest on the usual discretization of the cutter's edges into elemental cutting edge segments (Hong and Ehmann,1995). Each elemental cutting edge will be considered as an oblique cutting tool, therefore, the two dimensional orthogonal cutting force model can not be applied to model milling operations. Therefore, a three dimensional cutting force model will be developed by using oblique cutting test data.

3.1 Model Formulation

The instantaneous shear plane area will be taken as a measure of the force applied by the cutting tool

The Resultant Force on the Elemental Cutting Edges

The resultant force on the elemental cutting edge is the vector sum of force components. After neglecting the end force components the resultant force can be represented as:

$$\begin{aligned} \bar{R}_{i,j}(t) &= \bar{F}_{ci,j}(t) + \bar{F}_{ti,j}(t) + \bar{F}_{li,j}(t) \\ &= \bar{F}_{xi,j}(t) + \bar{F}_{yi,j}(t) + \bar{F}_{zi,j}(t) \end{aligned} \tag{7}$$

where $\bar{F}_{ci,j}(t)$, $\bar{F}_{ti,j}(t)$, and $\bar{F}_{li,j}(t)$ are the cutting, thrust, and lateral forces exerted on the periphery of the cutter.

On the other hand, the resultant cutting force is the sum of the force to shear the work material into chips and of the contact force:

$$\bar{R}_{i,j}(t) = \bar{R}_{2i,j}(t) + \bar{F}_{ii,j}(t) \tag{8}$$

where $\vec{R}_{2i,j}(t)$ is the resultant cutting force exerted by the elemental cutting edge to remove the chip and $\vec{F}_{ii,j}(t)$ is the corresponding contact force between the elemental cutting edge and the workpiece.

Considering the chip as a free body, $\vec{R}_{2i,j}(t)$ can be represented by the friction force $\vec{F}_{fi,j}(t)$ and the normal force on the tool face $\vec{F}_{ni,j}(t)$. From Fig. 3 we have:

$$\vec{F}_{ni,j}(t) = \vec{R}_{2i,j}(t)\cos\beta(t) \quad (9a)$$

$$\vec{F}_{fi,j}(t) = \vec{R}_{2i,j}(t)\sin\beta(t) \quad (9b)$$

where $\beta(t)$ is the instantaneous friction angle on the tool surface. In turn, the resultant force on the shear plane $\vec{R}_{1i,j}(t)$ can be represented by the shear force $\vec{F}_{si,j}(t)$ and the normal force $\vec{F}_{nsi,j}(t)$ on the shear plane.

The Resultant Cutting Force Model

Separating the resultant cutting force in Eq. 8 into the cutting and thrust components, which are parallel and perpendicular to the instantaneous cutting velocity, and the lateral force component perpendicular to the plane formed by $\vec{F}_{ci,j}(t)$ and $\vec{F}_{ti,j}(t)$, we have

$$F_{ci,j}(t) = F_{ni,j}(t)\cos\gamma_n\cos i + F_{fi,j}(t)\sin\gamma_n + F_{ifi,j} \quad (10a)$$

$$F_{ti,j}(t) = -F_{ni,j}(t)\sin\gamma_n + F_{fi,j}\cos\gamma_n\cos\eta_c + F_{ini,j} \quad (10b)$$

$$F_{li,j}(t) = -F_{ni,j}(t)\cos\gamma_n\sin i - F_{fi,j}(t)\cos\gamma_n\cos\eta_c \quad (10c)$$

3.2 Determination of Parameters Used in the Cutting Force Model

The use of Eq. 10 to calculate the cutting force components requires the knowledge of the parameters τ, β, $V(t)$, ϕ_e, and γ_e and of the contact force coefficients. A method to calculate the aforementioned parameters from measurements of cutter geometry and cutting test data for different workpiece materials will be discussed in Appendix. It will be assumed that the values of τ, β, ϕ_e, and γ_e remain constant during the process.

4. VERIFICATION OF THE FORCE MODEL

A number of cutting tests have been conducted to verify the feasibility of the proposed method and of the derived force model. Cutting force components were measured by a three-component dynamometer (Kistler type 9255B). The accelerations in the X, Y, and Z directions were measured by accelerometers (PCB type U353, UJ353, and 302A02) mounted on a specially machined aluminum cube attached to the spindle housing of the machining center. The workpiece was 6061 Aluminum.

The chip thickness was measured by using a Mitutoyo micrometer M820-25V with a ball tips on both ends. Two one-tooth cutters were used. One of them had a 38.1 mm (1.5 in.) diameter with a carbide insert with zero helix angle and flat cutting edge (zero rake angle) so that the milling operation with this cutter can be considered as an orthogonal cut. The other one was a 19.05 mm (0.75 in.) cutter made of High Speed Steel (HSS) with a 40^o helix angle and $\gamma_n = 15^o$. Three materials were used as the workpiece: AISI-1018 hot-rolled steel, free-machining alloy 360 brass, and 6061 Aluminum.

The cutting conditions were: feed = 3, 5, 15, 30, 45, and 60 mm/min, spindle speed = 100, 600, 1200 rpm, and width of cut = 0.5, 1, 2, 4, 6 mm, respectively. Table 1 shows the coefficients calculated from the measured cutting force data.

Table 1 Cutting Force Coefficients

	k_{1c} (KN/m)	k_{1t} (KN/m)	k_{2c} (MN/m²)	k_{2t} (MN/m²)
Al	2.2	2.85	304.11	317.33
Brass	1.78	2.12	209.23	100.69
Steel	1.45	2.11	420.42	246.18

The measured chip thickness data and calculated parameters are listed in Table 2.

Figures 3 to 5, which correspond to oblique cutting with the 40^o helix angle one tooth milling cutter, show the comparison between the measured and predicted cutting forces by using different force models. Model A is the shear plane based force model calculated by using Eqs. A6 and A7 in Appendix. Model B is the nominal undeformed chip thickness based force model calculated by using Eq. 4. Model D is the result of using the nominal undeformed chip thickness and penetration rate model given by Eq. 6. The forces based on models B and D were evaluated by using a simulation program with a similar architecture as the program for model A. The cutting conditions used were $b = 6mm$, $\omega = 600$ rpm, and $f_t = 0.05$ mm/tooth with the one-tooth helical cutter. The results prove the good predictive capability of the derived cutting force model especially with respect to the peak and average force predictions and the overall force shapes which are also in good agreement with the experimental data. They also show that the results of model A are closer to the experimental data than the results of models B and D. The errors in the average cutting forces calculated by using different models are listed in Table 3. It is evident that model A is consistently in better agreement with the measurements than the other models.

Table 2 Measured Chip Thickness and Calculated Cutting Parameters

	Steel	Brass	
t_c (mm)	0.146	0.057	0.113
ϕ_n (deg.)	19.95	47.63	25.77
γ_e (deg.)	34.41	34.41	34.41
η_s (deg.)	29.64	5.13	25.44
ϕ_e (deg.)	19.31	55.13	25.96
β (deg.)	49.63	44.98	65.50
τ (MN/m^2)	108.82	64.28	85.80

5. CONCLUSIONS

The following specific conclusions can be drawn:

(1) A cutting force model based upon the instantaneous shear plane area was derived and compared to other cutting force models. The results show that the shear plane based force model is physically sound and better represents the machining process.

(2) The proposed cutting force model was defined based on a discrete representation of the end milling process. The cutting edges of the milling cutter were divided into many segments, each considered as an oblique cutting edge. The resultant cutting forces were computed as the sum of the elemental cutting forces composed of a chip shearing and of a tool-workpiece contact force component.

(3) Algorithms for calculating the cutting process parameters used in the derived cutting force model were introduced.

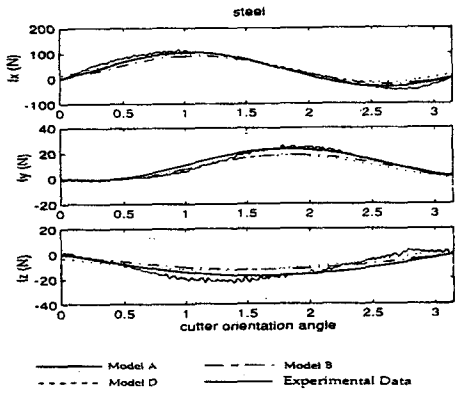

Fig. 3 Comparison of Measured and Predicted Cutting Forces – Steel

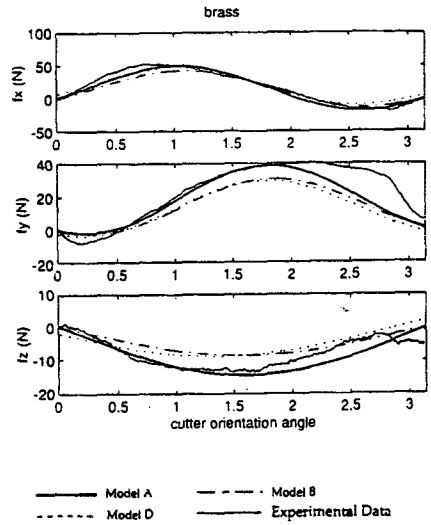

Fig. 4 Comparison of Measured and Predicted Cutting Forces – Brass

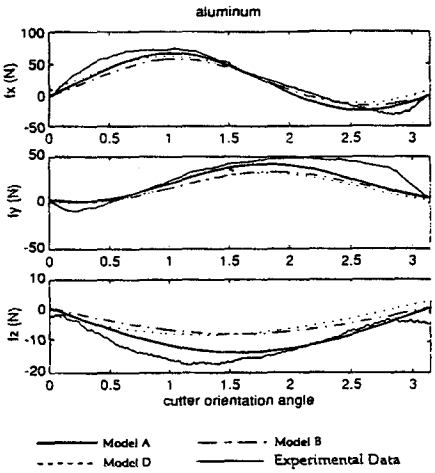

Fig.5 Comparison of Measured and Predicted Cutting Forces – Aluminum

REFERENCE

Albrecht, P., 1965, "Dynamics of the Metal Cutting Process," Journal of Engineering for Industry, Vol. 87, pp. 429-441.

Andrew, C., 1965, "Chatter in Horizontal Milling," Proc. Inst. Mech. Engrs., Vol. 79, pp. 877-906.

Armarego, E. J. A., and Epp, C., J., 1970, "An Investigation of Zero Helix Peripheral Up-Milling," Int. J. Mach. Tool Des. Res., Vol. 10, pp. 273-291.

Armarego, E. J. A., Wang, J., and Deshpande, N. P., 1995, "Computer-Aided Predictive Cutting Model for Forces in Face Milling Allowing for Tooth Runout," Annals of the CIRP, Vol. 44, pp. 43-49.

Hong, M. S. and Ehmann, K. F., 1995, "Generation of Engineered Surfaces by the Surface-Shaping System," Int. J. Mach. Tools Manufact., Vol. 35, pp. 1269-1290.

Lee, E. H. and Shafer, B. W., 1951, "The Theory of Plasticity Applied to a Problem of Machining," J. of Applied Mechanics, Vol. 18, No. 4, p. 405.

Merchant, M. E., 1944, "Basic Mechanics of the Metal Cutting Process," Trans ASME, Vol. 66, pp. 168-175.

Minis, I., Yanushevsky, R., and Tembo, A., 1990, "Analysis of Linear and Nonlinear Chatter in Milling," Annals of the CIRP. Vol. 39, pp. 459-462.

Shaw, M. C., 1991, *Metal Cutting Principle*, Oxford Science Publication.

Shaw, M. C., Cook, N., H., and Smith, P. A., 1952, "The Mechanics of Three dimensional Cutting Operations," Trans. ASME, Vol. 74, pp. 1055-1064.

Shin, Y. C. and Waters, A. J., 1994, "Face Milling Process Modeling with Structural Nonlinearity," Trans. of the NAMRI, pp. 157-163.

Tlusty, J. and Ismail, F., 1983, "Special Aspects of Chatter in Milling," Journal of Vibration, Acoustics, Stress, and Reliability in Design, Vol. 105, pp. 24-32.

Tobias, S. A., 1965, *Machine Tool Vibration*, Wiley, N.Y.

Usui, E., Hirota, A., and Masuko, M., 1978, "Analytical Prediction of Three Dimensional Cutting Process, Part 1 Basic Cutting Model and Energy Approach," Trans. ASME, Vol. 100, pp. 222-228.

APPENDIX :

The general procedure to evaluate the cutting process parameters on the shear plane is the following:

(1) Experimentally measure the cutting forces for different average undeformed chip thickness values. The average undeformed chip thickness is calculated as $2f_t/\pi$, where f_t is the feed per tooth.

(2) Measure the cutter helix angle η and normal rake angle γ_n.

Table 3 The Error Percentages for Average Cutting Forces for Different Models

	Model								
	A	B	D	A	B	D	A	B	D
	F_x			F_y			Fz		
Steel	3.54	6.32	6.01	2.66	3.85	3.90	5.20	8.89	8.72
Brass	2.96	5.16	5.09	4.11	9.94	9.88	8.65	20.11	19.97
Al	3.37	6.01	5.78	6.07	9.65	9.47	11.12	21.17	20.54

(3) Calculate the normal shear angle ϕ_n using Eq. A1 and the measured chip thickness ratio r_t.

$$\phi_n(t) = \tan^{-1}\left[\frac{r_t \cos\gamma_n(t)}{1 - r_t \sin\gamma_n(t)}\right] \quad \text{(A1)}$$

(4) The effective rake angle γ_e is obtained by Eqs. A2 and A3.

$$\eta_c = \cos^{-1}\left(\frac{b_c \cos i}{b}\right) \quad \text{(A2)}$$

$$\gamma_e(t) = \sin^{-1}[\sin\gamma_n(t)\cos i\cos\eta_c + \sin\eta_c \sin i] \quad \text{(A3)}$$

(5) The shear flow angle η_s is obtained by using Eq. A4.

$$\eta_s(t) = \tan^{-1}\left[\frac{\tan i\cos[\phi_n(t) - \gamma_n(t)] - \tan\eta_c \sin\phi_n(t)}{\cos\gamma_n(t)}\right] \quad \text{(A4)}$$

(6) The effective shear angle ϕ_e is calculated by using Eq. A5.

$$\phi_e(t) = \sin^{-1}\left[\frac{\cos\gamma_e(t)\cos\eta_s(t)}{\cos\eta_c\cos\gamma_n(t)}\sin\phi_n(t)\right] \quad \text{(A5)}$$

(7) To obtain the coefficients k_{2c} and k_{2t} the cutting and thrust forces are plotted versus the average undeformed chip thickness.

$$F_c = \frac{tA\cos(\eta_s - i)(\cos\beta\cos\gamma_n\cos i + \sin\beta\sin\gamma_n)}{\cos(\phi_e + \beta - \gamma_e)} + bk_{1c} \quad \text{(A6)}$$

$$F_t = \frac{tA\cos(\eta_s - i)(-\cos\beta\sin\gamma_n + \sin\beta\cos\gamma_n\cos\eta_c)}{\cos(\phi_e + \beta - \gamma_e)} + bk_{1t} \quad \text{(A7)}$$

By curve-fitting the data k_{2c} and k_{2t} are obtained as the slope of the lines. The contact force coefficients k_{1c} and k_{1t} correspond to the value of the cutting and thrust forces for a value of the undeformed chip thickness t = 0.

(8) The shear stress can be calculated by

$$\tau = \frac{(k_{2c}\cos\beta + k_{2t}\sin\beta)\cos(\phi_e + \beta - \gamma_e)\sin\phi_e}{coticos\gamma_n\cos(\eta_s - i)} \quad \text{(A8)}$$

where the friction angle β is given by

$$\beta = \tan^{-1}\left[\frac{\cos\gamma_n\cos i + \frac{k_{2c}}{k_{2t}}\sin\gamma_n}{\frac{k_{2c}}{k_{2t}}\cos\gamma_n\cos i - \sin\gamma_n}\right] \quad \text{(A9)}$$